Experimental Thermal and Fluid Science 66 (2015) 243–253

Contents lists available at ScienceDirect

Experimental Thermal and Fluid Science

journal homepage: www.elsevier.com/locate/etfs

Characteristics of gas–liquid two-phase flows through a sudden contraction in rectangular microchannels

Akimaro Kawahara [a,*], Mohamed H. Mansour [b], Michio Sadatomi [a], Wen Zhe Law [a], Hiroki Kurihara [a], Haslinda Kusumaningsih [c]

[a] Department of Mechanical System Engineering, Kumamoto University, Kurokami 2-39-1, Chuo-ku, Kumamoto 860-8555, Japan
[b] Department of Mechanical Power Engineering, Mansoura University, Egypt
[c] Department of Mechnical Engineering, Brawijaya University, Indonesia

ARTICLE INFO

Article history:
Received 10 January 2015
Received in revised form 14 March 2015
Accepted 14 March 2015
Available online 9 April 2015

Keywords:
Microchannel
Two-phase flow
Sudden contraction
Bubble velocity
Bubble length
Pressure change

ABSTRACT

A series of experiments were conducted to study the effects of contraction ratio and different liquid properties on gas–liquid two-phase flow through sudden contraction in micro-channel. Two rectangular microchannels with different contraction ratio were used. The widths of the larger channels upstream of the contraction were 0.53 or 0.78 mm (0.230 mm in height), while those of the smaller ones were fixed at 0.270 mm (0.230 mm in height). Distilled water, ethanol 49 wt% aqueous solution, pure ethanol and hydrofluoroether (HFE)-7200 were used as the test liquids, and nitrogen as the test gas. Flow pattern, bubble length, liquid slug length and bubble velocity were determined by analyzing video images of the flows. In addition, pressure profile upstream and downstream from the contraction was also measured for single-phase and two-phase flows. The pressure loss due to the contraction was determined from the pressure profiles. In the analysis, bubble velocity data and the pressure loss data were compared with calculations by some correlations in literatures. The bubble velocity data both upstream and downstream from the contraction were correlated with Kawahara et al.'s correlation (2010) where the correlation was accounted for aspect ratio of the channel. The correlation of the contraction coefficient for single-phase liquid flows was newly developed with Reynolds number and contraction ratio. The two-phase pressure drop data reasonably agreed with a slip flow model combined with the present contraction coefficient correlation and drift flux model based void fraction correlation. Moreover, numerical simulations were performed using the computational fluid dynamics software FLUENT (Fluent Inc.) and the volume of fluid (VOF) model. The present numerical simulation data agreed well with the experimental data for flow pattern, bubble velocity, bubble length, bubble pitch and pressure changes through the contraction.

1. Introduction

Two-phase flows across singularities such as bend, contraction and expansion are commonly seen in piping of many industrial systems and/or devices. With the advent of advance micro-processing technology, devices are down-sized and micro-devices are becoming more widespread, e.g., micro-reactors (Jähnisch et al. [1]), mobile-type fuel cell (Yen et al. [2]) and micro-heat exchangers (Qu and Mudawar [3]). Thus, it is essential for the development and design of micro-devices to understand the characteristics of two-phase flow through singularities [4,5]. For example, flow area changes, i.e., sudden contraction and sudden expansion might cause flow separation at the sharp edge. This separation might induce the flow pattern change and an irreversible pressure loss. The flow pattern change as well as the pressure loss affect the mass transfer and heat transfer performance in micro-reactors and micro-heat exchangers. Studies [6,7] have been conducted for two-phase gas–liquid flows in conventional sized channels with sudden contraction. On the other hand, several researchers [4,5,8,9] pointed out that the information on two-phase flow through contraction is limited for micro scale channels.

Pressure drop caused by abrupt flow area changes in small channels has been studied by Abdelall et al. [4]. Deionized water and air were used as two-phase flow mixture. The geometries of the abrupt channels were 1.6 mm and 0.84 mm for the larger and smaller inner diameter of pipe. The pressure drop data due to sudden contraction and/or expansion were affected by a

* Corresponding author. Tel./fax: +81 96 342 3753.
E-mail address: akimaro@mech.kumamoto-u.ac.jp (A. Kawahara).

http://dx.doi.org/10.1016/j.expthermflusci.2015.03.030
0894-1777/

significant velocity slip in the vicinity of the flow area change, and its values were lower than the prediction of the homogeneous model.

Chen et al. [8] had examined the two-phase flow characteristics across sudden contraction using air and water mixture. The contraction test section was from small rectangular channels (3×6 mm and 3×9 mm) into a small tube (3 mm). Their experimental data of pressure drop due to the contraction were compared with the calculations by homogeneous flow model recommended by Collier and Thome [10], Chisholm's correlation [6], Schmidt and Friedel correlation [7] and Abdelall et al.'s correlation [4]. The results from the homogeneous flow model are in good agreement with their data. Chen et al. [9] also had investigated the two-phase pressure drop across sudden contraction using air and water mixture. The contraction test section was from small rectangular channels (2×4 mm, 2×6 mm, 4×4 mm and 4×6 mm) into a small tube (2 mm). Based on their data, a modified homogeneous model was proposed to predict the pressure drop across the contraction.

From literature survey mentioned above, flow behaviors through sudden contraction in microchannel size less than 1 mm by using test liquid rather than water are not yet well understood. So, the purpose of this study is to investigate the effects of sudden contractions and liquid properties on gas–liquid two-phase flows in horizontal rectangular microchannel. In the experiments, two horizontal rectangular microchannels with contraction having different contraction ratio were used as the test channel. The widths of the larger channels upstream of the contraction were 0.53 or 0.78 mm (0.230 mm in height), while those of the smaller ones were fixed at 0.270 mm (0.230 mm in height). Distilled water, ethanol 49 wt% aqueous solution, pure ethanol and HFE-7200 were used as the test liquids, and nitrogen as the test gas. The pressure profile upstream and downstream of the contraction was also measured for single-phase and two-phase flows with pressure transducers. Data on the pressure loss due to the contraction were obtained from the pressure profiles. In addition, flow pattern and bubble velocity were determined by analyzing video images of the flows. In the analysis, the pressure loss data and bubble velocity data were compared with calculations by some correlations in literatures. Furthermore, this study attempts to develop a suitable numerical model using FLUENT for the two-phase flow in microchannel with sudden contraction.

2. Experiments

2.1. Test microfluidic chip

Fig. 1 shows a schematic diagram of the present microfluidic chips made of polydimethylsiloxane (PDMS). A rectangular microchannel with a sudden contraction was formed on the PDMS plate by photolithography and molding processes, and the inner wall surface of the channel has been treated by oxygen plasma to improve its wettability. By the treatment, the channel surface wettability has a similar one with glass. In our previous study [11], it is found that the bubble length trend in the present channel is similar with one in channels made of glass reported in literatures [12,13]. Table 1 shows the cross-sectional dimensions of two test channels with different contraction ratio σ_A ($= A_d/A_u$: area ratio of downstream channel to upstream one). Here, W and H are the width and height of the channel in upstream or downstream from the contraction, α^* the aspect ratio and D_H the hydraulic diameter. This chip had fourteen taps. Taps #1 and #2 were the liquid and the gas inlet ports. Thus, two phases were supplied through a T-junction type gas–liquid mixer. Taps #3 – #12 were connected to a pressure transducer, tap #14 was the gas–liquid mixture outlet to atmosphere. The distances between the mixer and pressure taps were $Z = Z_3 - Z_{12} = 4.5$, 7, 9.5, 12, 14.5, 19.5, 22, 24.5, 27, 29.5 mm, respectively. The detail of measurement for gas and liquid flow rates and pressure is referred to our previous study [15].

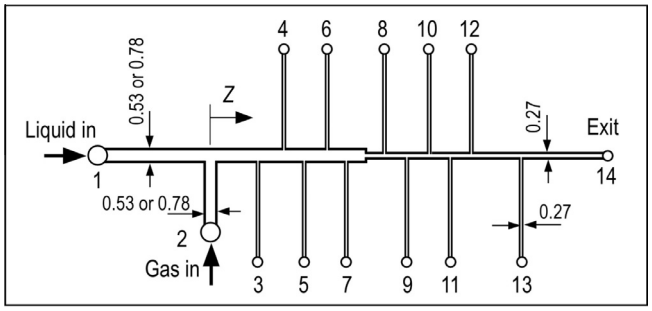

Fig. 1. Detail of test microfluidic chips.

The two-phase flows were observed with a high speed video camera (Hi-Dcam PCI 8000S, NAC Image Technology) in three observation areas, i.e., upstream ($Z = 17.5$ mm), contraction ($Z = 20.5$ mm) and downstream ($Z = 32.5$ mm). By using the recorded images, data on bubble length, L_G, and bubble velocity, u_G, were obtained. In addition, void fraction, α, was determined by substituting the u_G data and the gas volumetric flux, j_G, into $\alpha = j_G/u_G$.

The uncertainties of measured and calculated parameters mentioned above are shown in Table 2.

2.2. Data reduction

Fig. 2(a) and (b) show typical pressure distributions measured for HFE-7200 single-phase flow and nitrogen gas-HFE7200 two-phase flow. The ordinate is the gauge pressure, while the abscissa is the distance from the T-junction mixer. There are five pressure taps, tap #3 to tap #7 for upstream flow from the contraction and another five taps, tap #8 to tap #12 for downstream flow. The pressure taps provide the local gauge pressure along the upstream and downstream from the contraction. To obtain experimental data on pressure change due to the contraction, Δp_C, linear extrapolation of the axial pressure distribution was performed by calculating the difference of intersecting points at the sudden

Table 1
Cross-sectional dimensions of the test channels.

	Channel 1		Channel 2	
	Upstream	Downstream	Upstream	Downstream
$W \times H$ mm^2	0.53×0.23	0.27×0.23	0.78×0.25	0.27×0.25
$\alpha^* = H/W$	0.43	0.85	0.32	0.93
D_H mm	0.32	0.25	0.38	0.26
$\sigma_A = A_d/A_u$	0.51		0.35	

Table 2
Uncertainties of parameters measured in the present experiments.

Parameters	Maximum relative uncertainty (%)
Liquid flow rate	±2
Gas flow rate	±5
Pressure	±2
Bubble and liquid slug lengths	±5
Bubble velocity	±7
Void fraction	±10

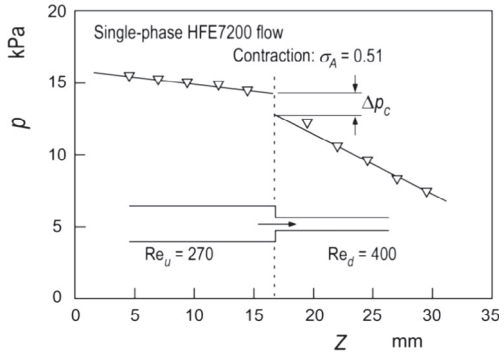

(a) Single-phase flow

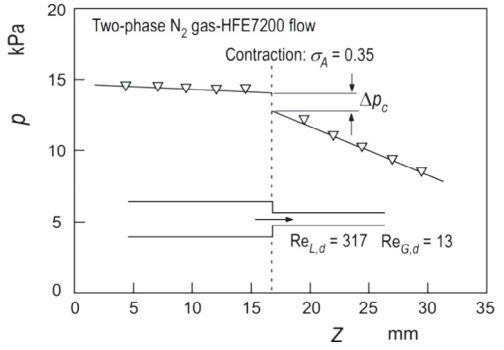

(b) Two-phase flow

Fig. 2. Pressure distribution along upstream and downstream from contraction. (a) Single-phase flow (b) Two-phase flow.

Table 3
Properties of test liquids.

Liquids	ρ_L (kg/m^3)	μ_L (mPa s)	σ (N/m)
Water	996.7 ± 1.9	0.919 ± 0.1	0.072 ± 0.001
Ethanol 49 wt%	911.2 ± 1.6	2.38 ± 0.15	0.028 ± 0.001
Ethanol	789.4 ± 3.4	1.23 ± 0.9	0.022 ± 0.001
HFE-7200	1433.9 ± 1.2	0.65 ± 0.1	0.014 ± 0.001

Table 4
Ranges of volumetric flux of liquid and gas. (a) σ_A = 0.51 (b) σ_A = 0.35.

Liquids	j_{Ld} (m/s)	j_{Gd} (m/s)
(a) σ_A = 0.51		
Water	0.20–0.57	0.30–0.75
Ethanol 49 wt%	0.11–0.24	0.28–0.73
Ethanol	0.12–0.35	0.29–0.76
HFE-7200	0.27–0.57	0.29–0.74
(b) σ_A = 0.35		
Ethanol 49 wt%	0.11–0.23	0.27–0.69
Ethanol	0.11–0.41	0.27–0.71
HFE-7200	0.21–0.55	0.26–0.69

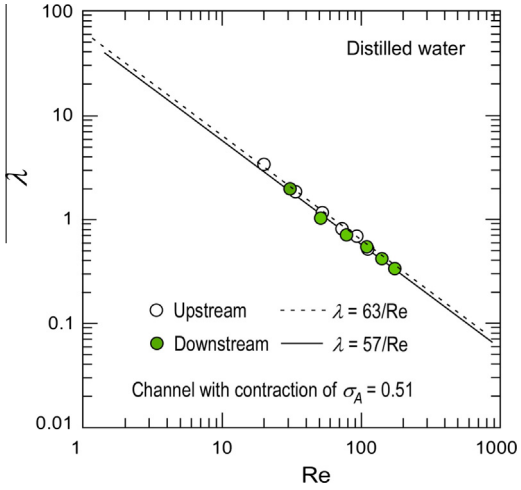

Fig. 3. Single-phase friction factors in straight channels upstream and downstream of the contraction.

contraction, as shown in Fig. 2(a) and (b). In the extrapolation, the pressure data at taps #7 and #8 have never been used to eliminate a peculiar change in pressure near the contraction position from linear pressure distribution.

In order to check the pressure measurement accuracy, the single-phase friction factors were determined from the upstream and the downstream fully developed pressure lines. Fig. 3 shows the Darcy friction factor data obtained for single-phase water flow in the present channel with a contraction ratio, σ_A = 0.51. The data are plotted against the Reynolds number, based on the hydraulic diameter. The open and solid symbols represent the friction factors measured in the upstream and the downstream channels, respectively. The data shown is in good agreement with the following classical theory by Shah and London [16] for laminar flow which is a function of aspect ratio, α^*, for a rectangular channel.

$$\lambda Re = 96(1 - 1.3553\alpha^* + 1.9467\alpha^{*2} - 1.7012\alpha^{*3} + 0.9564\alpha^{*4} - 0.2537\alpha^{*5}) \quad (1)$$

2.3. Flow conditions

Nitrogen gas was used as test gas, while distilled water, ethanol and hydrofluoroether (HFE) 7200 as test liquid. Table 3 shows properties of the test liquids, the density ρ, the dynamic viscosity μ and the surface tension σ. Table 4 shows the volumetric fluxes of liquid and gas in downstream channel with contractions of (a) σ_A = 0.51 and (b) σ_A = 0.35. The ranges of downstream dimensionless numbers defined by Eq. (2), i.e., Reynolds numbers and Weber numbers for liquid and gas, Bond number and capillary number, are shown in Table 5.

Table 5
Ranges of dimensionless numbers in the downstream channel. (a) σ_A = 0.51 (b) σ_A = 0.35.

Liquids	Re_L	Re_G	We_L	$We_G \times 10^4$	Bo	$Ca \times 104$
(a) σ_A = 0.51						
Water	55–160	5–13	0.14–1.1	3.7–24	0.009	2.5–7.1
Ethanol 49 wt%	9–17	5–13	0.10–0.46	8.9–58	0.02	12–26
Ethanol	20–56	5–13	0.13–1.1	12–77	0.022	6.7–19
HFE7200	16–340	5–13	1.9–8.5	19–121	0.062	12–25
(b) σ_A = 0.35						
Ethanol 49 wt%	8–18	5–13	0.09–0.45	8.2–53	0.021	11–25
Ethanol	19–68	5–13	0.11–1.5	11–69	0.023	6.0–23
HFE7200	126–317	5–13	1.2–7.9	16–108	0.067	9.5–25

$$Re_L = \frac{\rho_L j_{L,d} D_{H,d}}{\mu_L}, Re_G = \frac{\rho_G j_{G,d} D_{H,d}}{\mu_G}, We_L = \frac{\rho_L j_{L,d}^2 D_{H,d}}{\sigma},$$
$$We_G = \frac{\rho_G j_{G,d}^2 D_{H,d}}{\sigma}, \quad Bo = \frac{(\rho_L - \rho_G) g D_{H,d}^2}{\sigma}, Ca = \frac{\mu_L j_{L,d}}{\sigma} \tag{2}$$

3. Numerical simulations

3.1. Governing equations

The mass, momentum and gas volume fraction (α_G) conservation equations for an unsteady incompressible two-phase flow using Volume of Fluid (VOF) method can be written as

$$\frac{\partial \vec{V}}{\partial t} + \nabla \cdot (\rho \vec{V}) = 0 \tag{3}$$

$$\frac{\partial (\rho \vec{V})}{\partial t} + \nabla \cdot (\rho \vec{V} \vec{V}) = -\nabla p + \nabla \cdot \left\{ \mu (\nabla \vec{V} + \vec{V}^T) \right\} + \rho \vec{g} + \vec{F} \tag{4}$$

And

$$\frac{\partial \alpha_G}{\partial t} + \vec{V} \cdot \nabla \alpha_G = 0 \tag{5}$$

where ρ, μ, $\vec{V}$, p and $\vec{F}$ denote the mixture density, the mixture viscosity, the mixture velocity field, the pressure and the source term that represents the surface tension force, respectively. ρ, μ and $\vec{F}$ can be computed as a function of liquid and gas volume fractions (α_L and α_G),

$$\rho = \alpha_L \rho_L + \alpha_G \rho_G \tag{6}$$

$$\mu = \alpha_L \mu_L + \alpha_G \mu_G \tag{7}$$

$$\vec{F} = \sigma \frac{2 \rho k_G \nabla \alpha_G}{(\rho_G + \rho_L)} \tag{8}$$

k_G is the curvature computed from the divergence of the unit surface normal, and σ is the surface tension. The value of α_L and α_G should be between 0 and 1.

3.2. Model geometry

An unsteady two-phase (gas–liquid) flow was simulated through 3-D rectangular contraction microchannel to investigate the two-phase flow characteristics in the upstream, contraction and downstream sections, and the contraction coefficient and compare it with the experimental data. The dimensions of the tested microchannels are that studied experimentally and listed in Table 1. The geometry and mesh were generated in GAMBIT (Fluent Inc.) using hexahedral elements. A grid independence study was performed and it is found that the grids with 202524 and 277304 cells are fine enough and suitable for the calculations for area ratios of 0.35 and 0.51, respectively.

3.3. Numerical approach

Firstly, the microchannel was filled with liquid. Then, nitrogen and liquid were fed to the mixing channels. Two-phase flow is assumed unsteady and laminar. At the two inlets, uniform entrance volume flux is applied for the liquids and nitrogen, while at the exit, the pressure was assumed to be atmospheric. At the wall, a no-slip boundary condition was imposed. Also, simulations were performed in the FLUENT (Fluent Inc.) computational fluid dynamics package, which utilizes the finite volume method for the spatial discretization.

The Volume of Fluid (VOF) algorithm was implemented to model the gas–liquid flow through the sudden contraction in rectangular microchannels. VOF is a numerical technique which is used to track and locate the shape and position of the interface between two or more immiscible fluids. Moreover, the momentum equation, Eq. (4), along with the gas volume fraction (α_G) conservation equation, Eq. (5), is used to calculate α_G throughout the domain. The different phases can be identified by knowing the value of α_G (1 for gas phase, 0 for liquid phase and $0 < \alpha_G < 1$ for the interfaces). The interface is advected with the flow field through the numerical domain [17].

For all test cases, the interpolations for velocities and pressure are based on second order. The pressure–velocity coupling is obtained using the PISO (pressure-implicit with splitting of operators) scheme. The PRESTO! (pressure staggering option) and the geometric reconstruction schemes were used for the pressure and interface interpolation, respectively.

A segregated time dependent unsteady solver was used. Courant number was fixed at 0.25 and time step ranged between 1×10^{-5} and 1×10^{-6} s depending on the inlet volume flux to achieve the convergence of the solution. The wall contact angle of liquid is set to 0°.

4. Results and discussion

4.1. Flow pattern

Fig. 4 shows an example of flow images observed by experiment and numerical simulation for nitrogen gas-pure ethanol two-phase flow through a contraction with $\sigma_A = 0.51$. In the upstream of the contraction, shorter gas bubble whose length obeys Garstecki scaling law model [18] mentioned in Section 4.3., flows intermittently. This shorter gas bubble flow is called as the quasi-homogeous flow in our previous study [11,14,15]. In the downstream channel, quasi-separated flow, which is also intermittent flow of bubble and is characterized by longer gas bubbles surrounded by a smooth or wavy liquid film, can be observed. The bubble length for the quasi-separated flows is no longer followed by the scaling law model, as detailed in Section 4.3.

From Fig. 4(b), it is found that the present numerical simulation result offers an accurate representation of the experimental two-phase flow configuration with the same flow conditions.

4.2. Bubble velocity

Fig. 5 shows the bubble velocity data in the upstream channel with contraction of $\sigma_A = 0.51$. The data are plotted against the total volumetric flux, j ($= j_L + j_G$). The solid and broken lines represent respectively calculations by $u_G = j$ (homogeneous flow) and $u_G = 1.61j$ by the drift flux model of Zuber and Findlay [19].

$$u_G = C_0 j + V_{Gj} \tag{9}$$

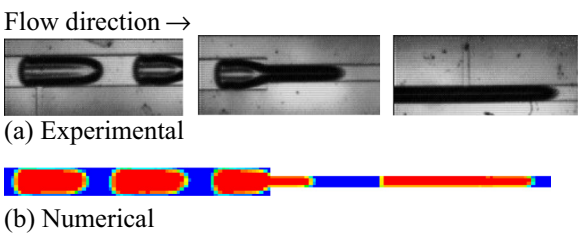

Fig. 4. Typical upside view for pure ethanol two-phase flow through sudden contraction $\sigma_A = 0.51$. (Flow rate condition: $j_{L,d} = 0.26$ m/s and $j_{G,d} = 0.48$ m/s). (a) Experimental (b) Numerical.

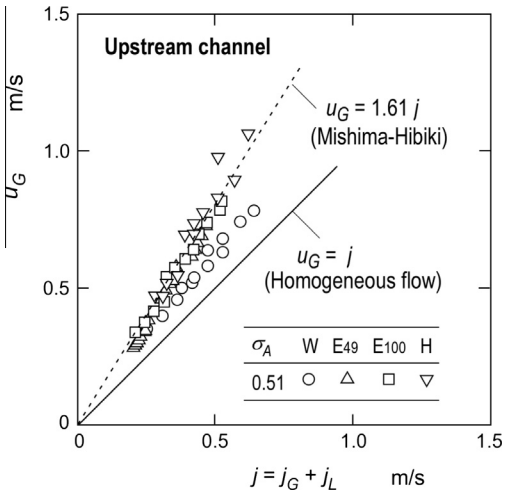

Fig. 5. Experimental data on bubble velocity in the upstream region of the test channel with $\sigma_A = 0.51$: Effects of liquid properties. (W: water, E_{49}: ethanol 49 wt% aqueous solution, E_{100}: pure ethanol, H: HFE-7200).

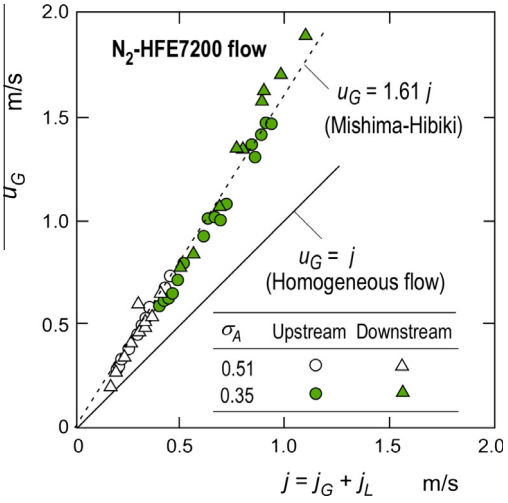

Fig. 6. Experimental data on bubble velocity for nitrogen gas-HFE7200 flows in the test channel with $\sigma_A = 0.51$ and 0.35.

Here, the drift velocity, V_{Gj} was taken as zero because of horizontal flow. The distribution parameter, C_0, was determined by Mishima-Hibiki's correlation [20].

$$C_0 = 1.2 + 0.510\exp(-0.691D) \tag{10}$$

Here, D is the inner diameter of tube in mm. The u_G data for all liquids are higher than the solid line, and those for HFE-7200, having both the lowest surface tension and viscosity, show the highest value.

Fig. 6 shows the u_G data for nitrogen gas-HFE-7200 in the upstream and the downstream channels with $\sigma_A = 0.51$ and 0.35. From the comparison of u_G between upstream and downstream channels, C_0 (= u_G/j) value is larger for the downstream than the upstream. In addition, form a comparison of u_G between $\sigma_A = 0.51$ and 0.35, the C_0 value is higher for $\sigma_A = 0.51$ than that for $\sigma_A = 0.35$. That is, C_0 increases with the channel aspect ratio.

In our previous study (Kawahara et al. [15]), we proposed the following C_0 correlation for square channel:

$$C_0 = aBo^{0.19}Re_L^{-0.01}We_G^{0.01} \tag{11}$$

In Eq. (11), a is a constant, Bo is the Bond number, Re_L the liquid Reynolds number and We_G the gas Weber number. By analyzing the present u_G data, the constant, a, can be correlated with aspect rato, α^*, as follows:

$$a = 3.46\alpha^{*0.23} \tag{12}$$

Fig. 7 shows the comparison of the bubble velocity between experiment and calculation by Eq. (9) together with Eqs. (11) and (12). Figs. (a) and (b) represent calculations respectively for upstream channel and downstream one of the contraction. The calculations agree with the data within root mean square errors of 20%, irrespective of aspect ratio, liquid properties as well as contraction ratio.

Fig. 8 shows a comparison of bubble velocity for contraction of $\sigma_A = 0.35$ between experiment and numerical simulation by VOF method described in Chapter 3. The numerical data reasonably agreed with experimental data for ethanol in both upstream and downstream of the contraction. On the other side, the numerical data apt to under-predict the experimental data for HFE-7200. The cause of the under-prediction is probably due to under-estimate liquid film thickness around the gas bubble by the present numerical simulation with VOF method as seen Fig. 10. The real shape of bubble nose and the bubble length is more shaper and longer than the numerical simulation results. Therefore, the real

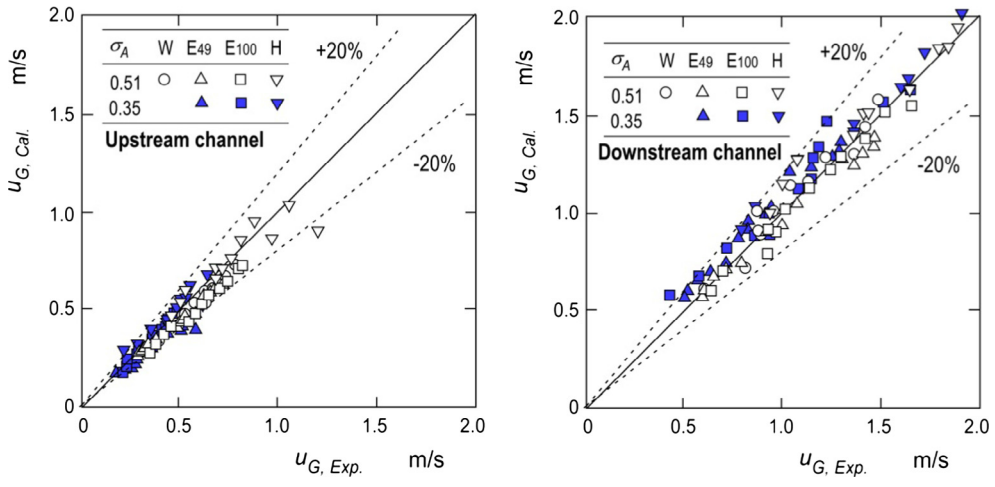

(a) Upstream channel (b) Downstream channel

Fig. 7. Comparison of bubble velocity between experiment and calculation by drift flux model with Kawahara et al.'s distribution parameter for the test channel with $\sigma_A = 0.51$. (a) Upstream channel (b) Downstream channel.

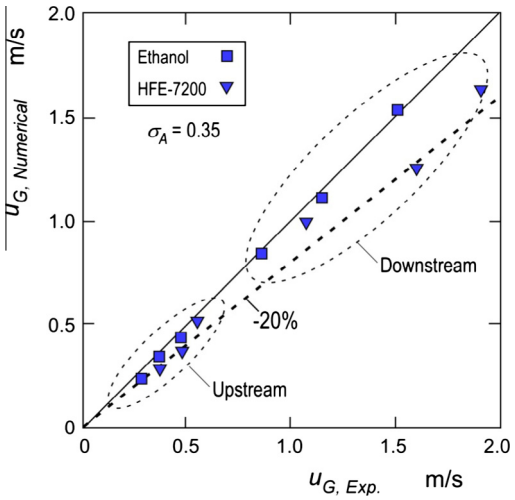

Fig. 8. Comparison of bubble velocity between experimental data and numerical data by simulation with VOF method.

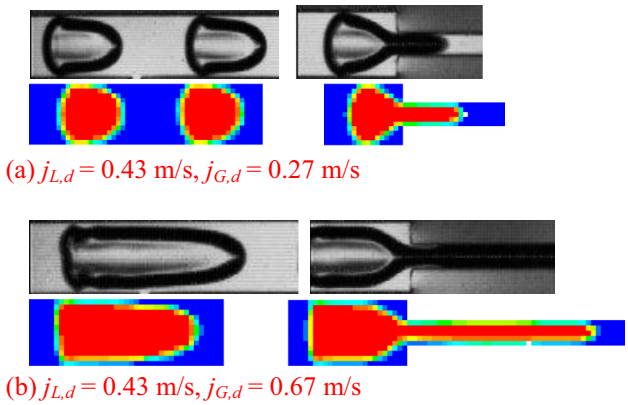

Fig. 9. Comparison of bubble shape between experiments and numerical results by VOF method (Nitrogen – HFE-7200 two-phase flows in the test channel with contraction of σ_A = 0.35.) (a) $j_{L,d}$ = 0.43 m/s, $j_{G,d}$ = 0.27 m/s (b) $j_{L,d}$ = 0.43 m/s, $j_{G,d}$ = 0.67 m/s.

bubble could move faster in central region of the channel. The liquid film thickness might depend on the liquid physical properties. Further studies are needed to know which the film thickness depend mainly on properties of such as higher density, lowest surface tension and dynamic viscosity of HFE-7200. Also, we can notice that the differences between the experimental and numerical data for HFE are relatively small at the upstream and at small values of $(j_L + j_G)$ downstream. In the numerical simulation, the value of j_L is considered constant. So, when increasing the values of j_G, the values of $(j_L + j_G)$ increase. Therefore, the bubble lengths increase and in the numerical simulations and due to the small value of the surface tension of HFE-7200, the gas bubbles were broken after the contraction section. The bubble velocity decreases with decreasing the bubble length due to the reduction of the liquid velocity ($u_L = j_L/(1 - \alpha_G)$). Also, this phenomenon was observed at the experiments at high values of j_G but may be due to the nature of the sudden contraction section in the experiments, the experimental bubble lengths after broken are greater than that in the numerical simulations.

4.3. Bubble length

Fig. 10 shows the dimensionless bubble length data, L_G/w, by the channel width, w. The abscissa is the ratio of the gas volume flow rate to the liquid one, Q_G/Q_L. The solid curve represents calculation by Garstecki et al.'s [18] correlation:

$$\frac{L_G}{w} = 1 + \frac{Q_G}{Q_L} \tag{13}$$

In the upstream as shown in Fig. 10(a), the data for the quasi-homogeneous flow distribute around calculations by Eq. (13), irrespective of liquid properties. On the other side, the data for quasi-separated flow take a much higher value than the solid line. In the downstream as shown in Fig. 10(b), the bubble length increases after passing through the contraction and takes higher value than the calculation by Garstecki et al.'s correlation, depending on the contraction ratio. Assuming constant bubble volume at both upstream and downstream, and neglecting the liquid film thickness between the bubble and the channel wall, the bubble length can be calculated by the following equation,

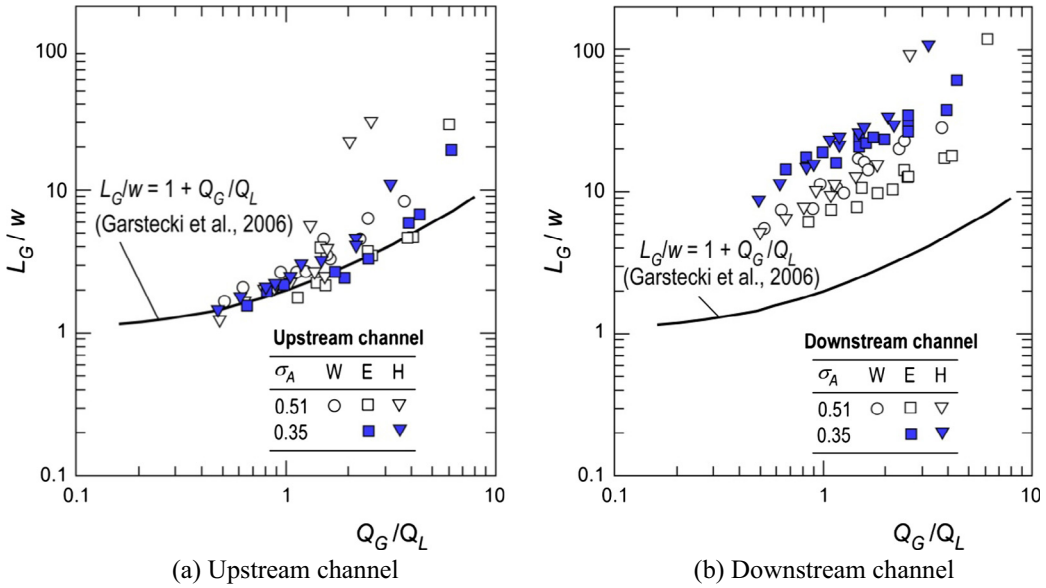

(a) Upstream channel (b) Downstream channel

Fig. 10. Dimensionless bubble length data plotted against gas–liquid volume flow rate ratio. (a) Upstream channel (b) Downstream channel.

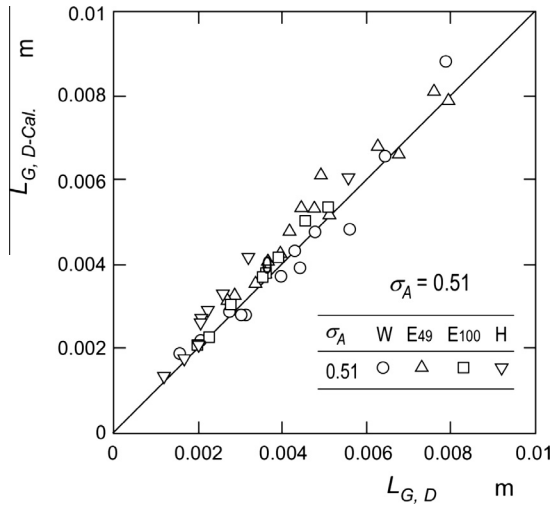

Fig. 11. Relation between $L_{G,d}$ and $L_{G,d\text{-}cal}$ for the test channel with contraction of $\sigma_A = 0.51$.

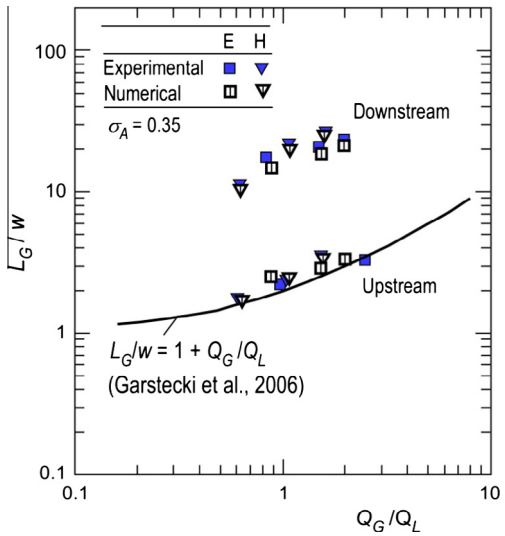

Fig. 12. Numerical simulation results for bubble length in upstream and downstream of contraction with $\sigma_A = 0.35$. (E: pure ethanol, H: HFE-7200).

$$L_{G,d-cal} = \frac{L_{G,u}A_u}{A_d} \tag{14}$$

Here, A_u and A_d are the cross-sectional areas of the channels in the upstream and the downstream. Fig. 11 shows the comparison between the experimental $L_{G,d}$ and calculated $L_{G,d\text{-}cal}$. The results of $L_{G,d\text{-}cal}$ agree with $L_{G,d}$, irrespective of kinds of the test liquids. Thus, the increase in the bubble length is not caused by the coalescence of bubbles, but by extension of bubble due to reduction of flow area.

Fig. 12 shows comparsion of L_G/w between experiment and numerical simulation for contraction with $\sigma_A = 0.35$. The numerical simulation results agree qualitatively and quatitavely with experimental one for both ethanol and HFE-7200 case in upstream and downstream of the contraction.

Fig. 13(a) and (b) show the relation between the ratio of bubble length to unit cell length L ($= L_G + L_L$; L_L is the liquid slug length) and homogeneous void fraction β ($= j_G/(j_G + j_L)$) for upstream and downstream regions. The solid curve shows the calculation by Kawahara et al. emprical correlation [17].

$$\frac{L_G}{L} = \frac{0.9\beta^{0.68}}{1 - 0.1\beta^{0.005}} \cong \beta^{0.68} \tag{15}$$

This correlation was based on the L_G/L data obtained for a horizontal straight square and circular microchannels. The data for the upstream and downstream channels distribute close to the curve. Therefore, there is no effect of the contraction ratio as well as the channel aspect ratio.

Fig. 14 shows numerical simulation results for L_G/L in the upstream and downstream of the contraction with $\sigma_A = 0.35$. The numerical simulation results showed the same trend with the experimental results and/or emprical correlation, Eq. (15).

4.4. Pressure change across contraction

The total pressure change across sudden contraction, Δp_C, consists of the irreversible and reversible pressure drop, and could be expressed by the following equation:

$$\Delta p_C = \frac{\rho u_d^2}{2}(K_C + 1 - \sigma_A) \tag{16}$$

$$K_C = \left(1 - \frac{1}{C_C}\right)^2 \tag{17}$$

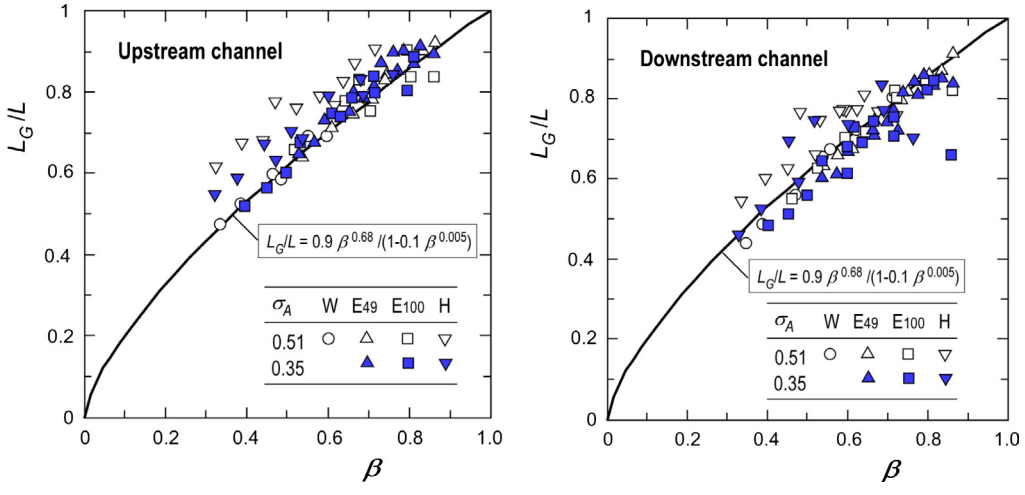

(a) Upstream channel (b) Downstream channel

Fig. 13. Experimental data on ratio of bubble length to unit cell length plotted against homogeneous void fraction. (a) Upstream channel (b) Downstream channel.

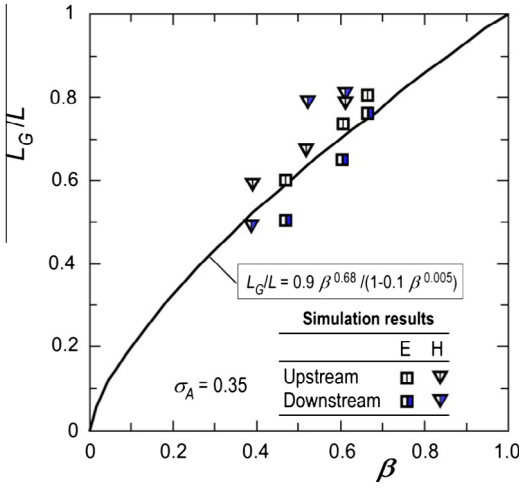

Fig. 14. Numerical simulation results for L_G/L in upstream and downstream of the contraction with $\sigma_A = 0.35$.

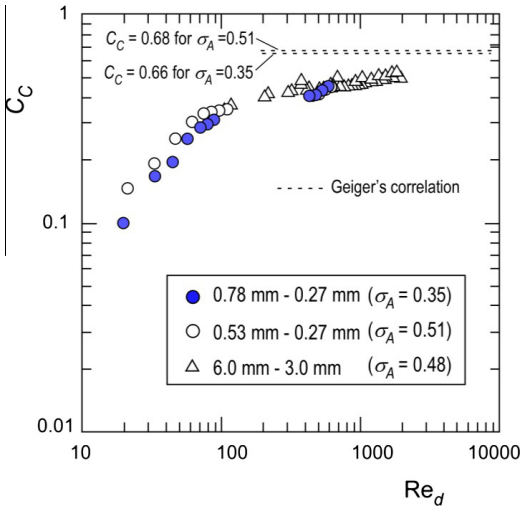

Fig. 15. Contraction coefficient for single-phase liquid flows in micro- and mini-channels.

Here, ρ is the density of working fluid, u_d the velocity in the downstream, K_C the contraction loss coefficient and C_C the contraction coefficient. Fig. 15 shows the present C_C data against Reynolds number in downstream, Re_d. The data in mini-channel (Sadatomi et al. [21]), which is a rectangular one having $W = 6$ mm to 3 mm, are also plotted. Dotted lines show the calculation by Geiger's [22] correlation:

$$C_C = 1 - \frac{1-\sigma_A}{2.08(1-\sigma_A)+0.5371} \tag{18}$$

The C_C data for mini- and micro-channels increase with the Reynolds number, and were correlated with the following equation:

$$C_C = B + (1-B)\sigma_A^{4.519}, B = 0.0645\ln Re_d - 0.00792 \tag{19}$$

Fig. 16 shows comparison of C_C between experiment and calculation by Eq, (19). The calculation agrees with the data within RMS errors of 10%, except for some data points, which are collected in very low Reynolds number.

Fig. 17(a) and (b) show the experimental data on pressure change due to the contraction, Δp_C, respectively for contraction

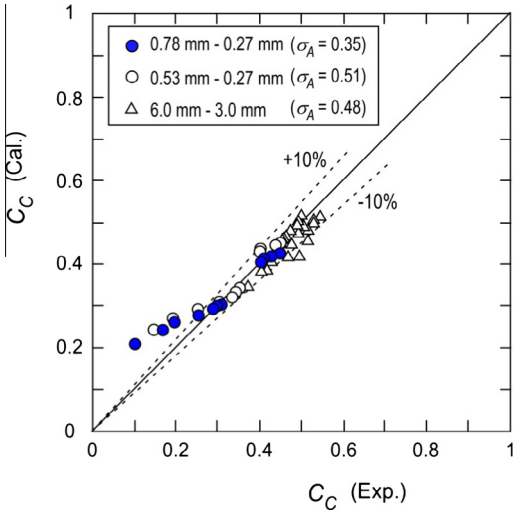

Fig. 16. Comparison of contraction coefficient between experiment and calculation by the present empirical correlation.

ratios $\sigma_A = 0.51$ and 0.35. The data are plotted against the total volumetric flux in the downstream of the contraction. The Δp_C value increases with the total volumetric flux, irrespective of σ_A. In addition, the Δp_C value is the highest for HFE-7200 which has the highest density and the lowest viscosity and surface tension.

The present experimental Δp_C data were compared with models and/or correlations in literature, i.e., Chisholm [6], Schmidt and Friedel [7], Abdelall et al. [4], Collier and Thome [10], listed in Table 6. Table 6 also shows the comparison results, regarding root mean-square error, $\varepsilon_{RMS} = \sqrt{\frac{1}{N-1}\sum\left(\frac{\Delta p_{C,Cal}-\Delta p_{C,Exp}}{\Delta p_{C,Exp}}\right)^2}$. Of four correlations, prediction by Chisholm's correlation is the best for $\sigma_A = 0.35$, while Abdelall et al.'s one for $\sigma_A = 0.51$. The Chisholm's correlation is ba sed on homogeneous flow model and expressed as

$$\Delta p_C = \frac{G_d^2}{2\rho_L}\left\{\frac{1}{(\sigma_A C_C)^2} - 1 - \frac{2\left(\frac{1}{C_C}-1\right)}{\sigma_A^2}\right\}\left\{1 + x\left(\frac{\rho_L}{\rho_G}-1\right)\right\} \tag{20}$$

Here, G_d is the total mass flux in downstream channel and x is the mass quality. Chisholm [6] also proposed the following correlation as contraction coefficient C_C:

$$C_C = \frac{1}{0.639(1-\sigma_A)^{0.5}+1} \tag{21}$$

The Abdelall et al.'s correlation [4] was developed based on their data obtained for sudden contraction consisting of larger tube (1.6 mm I.D.) and smaller tube (0.84 mm I.D.) and its contraction ratio of $\sigma_A = 0.28$.

$$\Delta p_C = \frac{G_d^2}{2\rho_L}\left\{\left(\frac{1}{C_C}-1\right)^2 + (1-\sigma_A^2)\right\}\phi_{C,L}^2 \tag{22}$$

$$\phi_{C,L}^2 = 120 X_M (X_M Re_L)^{-0.7} \tag{23}$$

$$X_M = \left(\frac{\mu_L}{\mu_G}\right)^{0.1}\left(\frac{1-x}{x}\right)^{0.9}\left(\frac{\rho_G}{\rho_L}\right)^{0.1} \tag{24}$$

Fig. 18(a) and (b) show comparison results respectively for Chisholm's correlation and Abdelall et al.'s one.

Abdelall et al. [4] also reported that their measured two-phase pressure changes due to sudden contraction indicated the occurrence of significant velocity slip between liquid and gas phases.

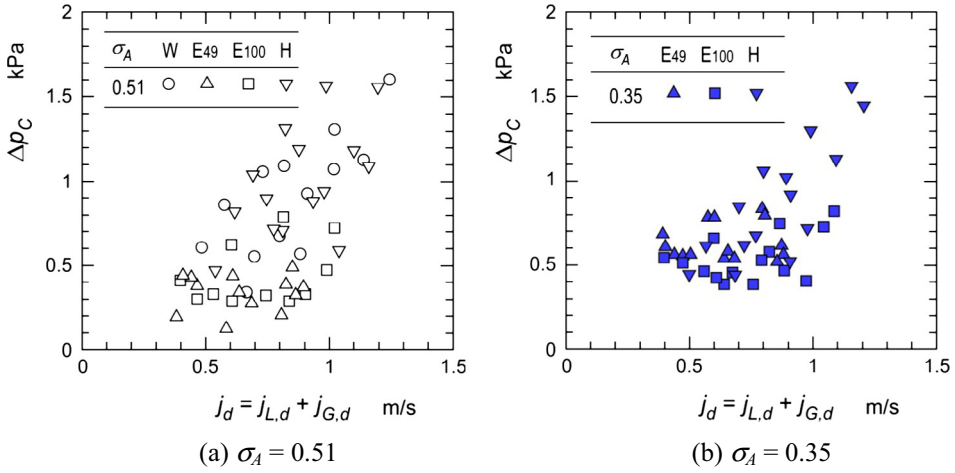

Fig. 17. Experimental data on two-phase pressure change across the sudden contraction plotted against total volumetric flux in the downstream channel. (a) $\sigma_A = 0.51$ (b) $\sigma_A = 0.35$.

Table 6
Root mean square errors of four correlations for prediction of Δp_C. (a) $\sigma_A = 0.51$ (b) $\sigma_A = 0.35$.

Correlations	Distilled water E_{RMS} (%)	Ethanol 49 wt% E_{RMS} (%)	Pure ethanol E_{RMS} (%)	HFE-7200 E_{RMS} (%)	All of liquids E_{RMS} (%)
(a) $\sigma_A = 0.51$					
Collier & Thome	86.19	88.11	90.15	77.48	85.48
Chisholm	44.27	49.26	52.25	30.87	44.16
Schmidt & Friedel	90.51	94.28	95.26	83.62	90.92
Abdelall et al.	56.64	92.82	40.16	37.32	56.73

Correlations	Ethanol 49 wt% E_{RMS} (%)	Pure ethanol E_{RMS} (%)	HFE-7200 E_{RMS} (%)	All of Liquids E_{RMS} (%)
(b) $\sigma_A = 0.51$				
Collier & Thome	93.60	86.26	70.42	83.43
Chisholm	46.33	78.64	183.08	102.68
Schmidt & Friedel	97.22	90.87	77.73	88.61
Abdelall et al.	54.35	71.97	40.70	55.67

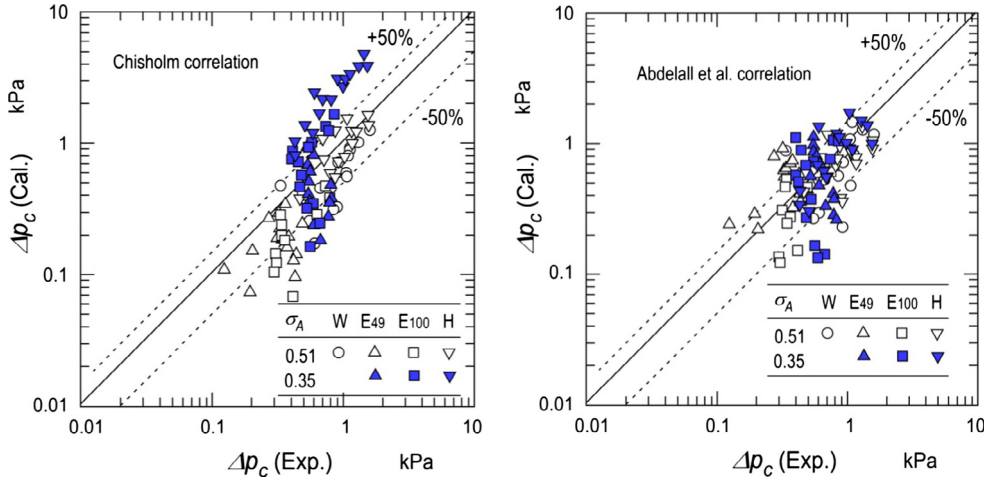

(a) Chisholm correlation (b) Abdelall et al. correlation

Fig. 18. Comparison of Δp_C between experiment and calculation by correlations in literatures. (a) Chisholm correlation (b) Abdelall et al. correlation .

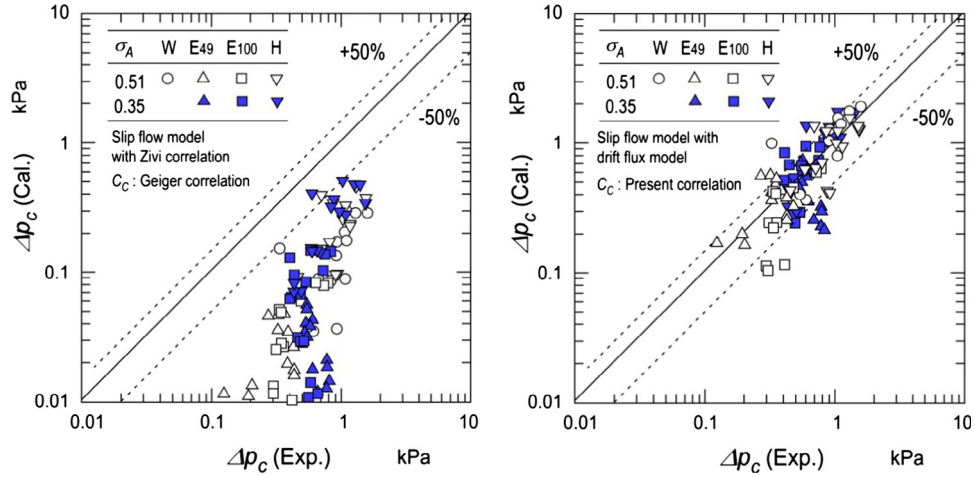

(a) Zivi correlation and Geiger correlation

(b) Drift flux model and present C_C correlation

Fig. 19. Comparison of Δp_C between experiment and calculation by slip flow model. (a) Zivi correlation and Geiger correlation (b) Drift flux model and present C_C correlation.

Table 7
Root mean square errors of slip flow model for prediction of Δp_C. (a) $\sigma_A = 0.51$ (b) $\sigma_A = 0.35$.

C_C/void fraction	Distilled water E_{RMS} (%)	Ethanol 49 wt% E_{RMS} (%)	Pure ethanol E_{RMS} (%)	HFE-7200 E_{RMS} (%)	All of liquids E_{RMS} (%)
(a) $\sigma_A = 0.51$					
Gieger/Zivi	87.22	94.69	94.57	78.67	88.79
Present/drift flux model	59.38	46.85	40.44	35.68	45.59

C_C/void fraction	Ethanol 49 wt% E_{RMS} (%)	Pure ethanol E_{RMS} (%)	HFE-7200 E_{RMS} (%)	All of liquids E_{RMS} (%)
(b) $\sigma_A = 0.35$				
Gieger/Zivi	97.90	89.58	73.93	87.14
Present/drift flux model	43.86	57.45	44.14	48.48

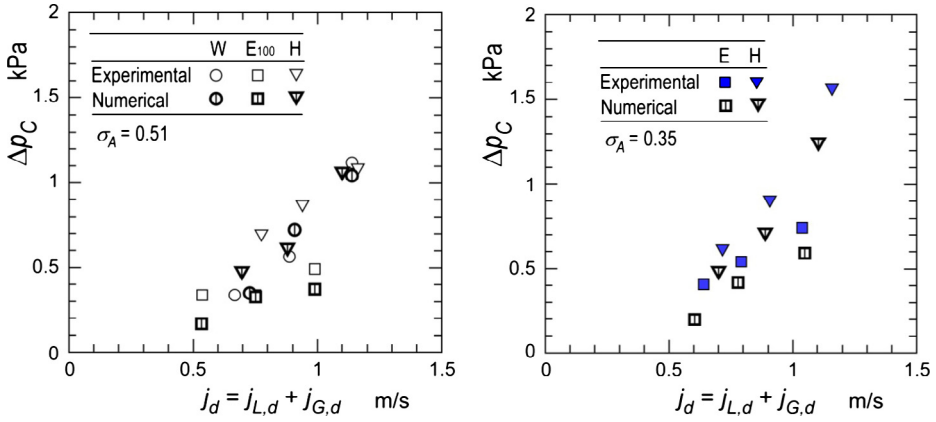

(a) $\sigma_A = 0.51$

(b) $\sigma_A = 0.35$

Fig. 20. Numerical simulation results for pressure change due to sudden contraction. (W: water, E100: pure ethanol, H: HFE-7200). (a) $\sigma_A = 0.51$ (b) $\sigma_A = 0.35$.

After that, they applied the following slip flow model based equation to predict their data.

$$\Delta p_C = G_d^2 \left\{ \frac{\rho_H \left(\frac{1}{C_C^2} - \sigma_A^2 \right)}{2\rho''^2} + \frac{(1 - C_C)}{\rho'} \right\} \tag{25}$$

$$\rho_H = \frac{\rho_L}{1 + x\left(\frac{\rho_L}{\rho_G} - 1\right)} \tag{26}$$

$$\rho' = \frac{(1-x)^2}{\rho_L(1-\alpha)} + \frac{x^2}{\rho_G \alpha} \tag{27}$$

$$\rho'' = \frac{(1-x)^3}{\rho_L^2(1-\alpha)^2} + \frac{x^3}{\rho_G^2\alpha^2} \tag{28}$$

$$\alpha = \frac{1}{(1-x)\frac{\rho_G}{\rho_L}S + 1} \tag{29}$$

Here, ρ_H is the homogeneous density and S is the slip ratio. As for S, Abdelall et al. [4] recommended Zivi's correlation [23] as follows:

$$S = (\rho_L/\rho_G)^{1/3} \tag{30}$$

They also recommended the use of Geiger's equation, Eq. (18), as contraction coefficient, C_C. Fig. 19(a) shows a comparison of Δp_C between experiment and calculation by the slip flow model with Eqs. 25–30 and Eq. (18). The calculation tends to under-predict the present data. As a trial, we calculated the pressure change by slip flow model with Eq. (19) as C_C and drift flux model, Eq. (9) together with Eqs. (11) and (12) as void fraction, and compared the calculation with the present data. Fig. 19(b) shows comparison results. The agreement between experiment and calculation becomes much better, irrespective of test liquids and contraction ratios. Table 7(a) and (b) lists the RMS relative errors of slip flow models with different contraction correlation and void fraction correlation mentioned above.

Fig. 20 shows the present numerical simulation results on Δp_C for contraction ratio with $\sigma_A = 0.51$ and 0.35. From the figure, it is found that the simulation data can capture qualitatively and quantitatively the present experimental data for $\sigma_A = 0.51$. On the other side, the simulation data for $\sigma_A = 0.35$ tend to under-predict the experimental data with −20%. The under-prediction might be caused by the under-estimation of bubble velocity as shown in Fig. 9.

5. Conclusions

The two-phase flows across the sudden contraction in horizontal rectangular microchannels have been studied experimentally and numerically. Main findings are as follows:

- Quasi-homogeneous and quasi-separated flow patterns are observed under the present flow conditions.
- The bubble length, L_G, data follow the Garstecki et al.'s correlation [18] for the quasi-homogeneous flow in the upstream channels. On the other hand, the data in the downstream one take much higher value than calculations by the Garstecki et al.'s correlation.
- There is no effect of the contraction on the ratio of bubble length to bubble pitch, L_G/L, data and the Kawahara et al.'s correlation [11] can be applied to the data, irrespective of channel aspect ratio.
- The bubble velocity is higher for the downstream channel than the upstream one, and depends on the liquid properties as well as channel aspect ratio. The bubble velocity data were correlated with well-known drift flux model [19] with modified one by Kawahara et al. [15] distribution parameter correlation by accounting for the aspect ratio.
- Total pressure drop across sudden contraction increased as total downstream superficial velocity increased.
- HFE-7200 and distilled water, which are higher in density showed higher pressure drop across sudden contraction.
- The empirical correlation of the contraction coefficient for single-phase liquid flows was newly developed with Reynolds number and contraction ratio.
- The two-phase pressure change experimental data reasonably agreed with calculations by a slip flow model with the present contraction coefficient correlation and drift flux void fraction correlation.
- The present numerical simulation data agreed well with the experimental data for flow pattern, bubble velocity, bubble length, bubble pitch and pressure changes through the contraction.

Acknowledgments

The authors wish to express their gratitude to Mr. S. Kawazoe for his cooperation in this experiment. The authors are grateful to the Egyptian Government for sponsoring M. H. Mansour. The present study was partially supported by KAKENHI (26420118).

References

[1] K. Jähnisch, M. Baerns, V. Hessel, W. Ehrfeld, V. Haverkamp, H. Lowe, Ch. Wille, A. Guber, Direct fluorination of toluene using elemental fluorine in gas/liquid microreactors, J. Fluorine Chem. 105 (2000) 117–128.
[2] T.J. Yen, N. Fang, X. Zhang, G.Q. Lu, C.Y. Wang, A micro methanol fuel cell operating at near room temperature, Appl. Phys. Lett. 83 (2003) 4056–4058.
[3] W. Qu, I. Mudawar, Flow boiling heat transfer in two-phase microchannel heat sinks –II. Annular two-phase flow model, Int. J. Heat Mass Transfer 46 (2003) 2773–2784.
[4] F.F. Abdelall, G. Hahm, S.M. Ghiaasiaan, S.I. Abdel-Khalik, S.S. Jeter, M. Yoda, D.L. Sadowski, Pressure drop caused by abrupt flow area changes in small channels, Exp. Thermal Fluid Sci. 29 (2005) 425–434.
[5] T.Y. Chalfi, S.M. Ghiaasiaan, Pressure drop caused by flow area changes in capillaries under low flow conditions, Int. J. Multiphase Flow 34 (2008) 2–12.
[6] D. Chisholm, Two-Phase Flow in Pipelines and Heat Exchangers, George Godwin, London and New York, 1983.
[7] J. Schmidt, L. Friedel, Two-phase flow pressure drop across sudden contractions in duct areas, Int. J. Multiphase Flow 23 (2) (1997) 283–299.
[8] I.Y. Chen, M.-C. Chu, J.-S. Liaw, C.-C. Wang, Two-phase flow characteristics across sudden contraction in small rectangular channels, Exp. Thermal Fluid Sci. 32 (2008) 1609–1619.
[9] I.Y. Chen, C.-Y. Tseng, Y.-T. Lin, C.-C. Wang, Two-phase flow pressure change subject to sudden contraction in small rectangular channels, Int. J. Multiphase Flow 35 (2009) 297–306.
[10] J.G. Collier, J.R. Thome, Convective Boiling and Condensation, Clarendon Press, Oxford, 1994.
[11] A. Kawahara, M. Sadatomi, S. Shimokawa, Lengths of bubble and slug and pressure drop in gas-liquid slug flow in microchannels, Multiphase Sci. Technol. 24 (3) (2012) 239–256.
[12] D.M. Fries, F. Trachsel, P.R. von Rohr, Segmented gas–liquid flow characterization in rectangular microchannels, Int. J. Multiphase Flow 34 (2008) 1108–1118.
[13] P. Sobieszuk, P. Cyganski, R. Pohorecki, Bubble lengths in the gas-liquid Taylor flow in microchannels, Chem. Eng. Res. Des. 88 (2010) 263–269.
[14] A. Kawahara, M. Sadatomi, K. Nei, H. Matsuo, Experimental study on bubble velocity, void fraction and pressure drop for gas-liquid two-phase flow in a circular microchannel, Int. J. Heat Fluid Flow 30 (2009) 831–841.
[15] A. Kawahara, M. Sadatomi, K. Nei, H. Matsuo, Characteristics of two-phase flows in a rectangular microchannel with a T-junction type gas-liquid mixer, Heat Transfer Eng. 32 (2011) 585–594.
[16] R.K. Shah, A.L. London, Laminar Flow Forced Convection in Ducts, Academic Press, New York, 1978.
[17] ANSYS FLUENT User's Guide: ANSYS Inc.
[18] P. Garstecki, M.J. Fuerstman, H.A. Stone, G.M. Whiteside, Formation of droplets and bubbles in a microfluidic T-junction – Scaling and mechanism of break-up, Lab Chip 2 (2006) 437–446.
[19] N. Zuber, J.A. Findlay, Average volumetric concentration in two-phase flow system, Trans. ASME J. Heat Transfer 87 (1968) 453–468.
[20] K. Mishima, T. Hibiki, Some characteristics of air-water two-phase flow in small diameter vertical tubes, Int. J. Multiphase Flow 22 (1996) 703–712.
[21] M. Sadatomi, S. Miyagawa, S. Santoso, A. Kawahara, Air-water two-phase flow through U-bend, sudden expansion and sudden contraction in rectangular mini-channels, WIT Trans. Eng. Sci. 79 (2013) 6375.
[22] G.E. Geiger, Sudden Contraction Losses in Single and Two-Phase Flow, Ph.D. Thesis, University of Pittsburgh, 1964.
[23] S.M. Zivi, Estimation of steady state steam void-fraction by means of principle of minimum entropy production, ASME Trans. Series C 86 (1964) 237–252.